Environmental Science & Technology

Article

pubs.acs.org/est

Impacts of Diffusive Transport on Carbonate Mineral Formation from Magnesium Silicate-CO_2-Water Reactions

Daniel E. Giammar,*[,†] Fei Wang,[†] Bin Guo,[§] J. Andrew Surface,[‡,∥] Catherine A. Peters,[§] Mark S. Conradi,[‡] and Sophia E. Hayes[‡]

[†]Department of Energy, Environmental and Chemical Engineering, Washington University, St. Louis, Missouri 63130, United States

[‡]Department of Chemistry, Washington University, St. Louis, Missouri 63130, United States

[§]Department of Civil and Environmental Engineering, Princeton University, Princeton, New Jersey 08544, United States

ABSTRACT: Reactions of CO_2 with magnesium silicate minerals to precipitate magnesium carbonates can result in stable carbon sequestration. This process can be employed in ex situ reactors or during geologic carbon sequestration in magnesium-rich formations. The reaction of aqueous CO_2 with the magnesium silicate mineral forsterite was studied in systems with transport controlled by diffusion. The approach integrated bench-scale experiments, an in situ spectroscopic technique, and reactive transport modeling. Experiments were performed using a tube packed with forsterite and open at one end to a CO_2-rich solution. The location and amounts of carbonate minerals that formed were determined by postexperiment characterization of the solids. Complementing this ex situ characterization, ^{13}C NMR spectroscopy tracked the inorganic carbon transport and speciation in situ. The data were compared with the output of reactive transport simulations that accounted for diffusive transport processes, aqueous speciation, and the forsterite dissolution rate. All three approaches found that the onset of magnesium carbonate precipitation was spatially localized about 1 cm from the opening of the forsterite bed. Magnesite was the dominant reaction product. Geochemical gradients that developed in the diffusion-limited zones led to locally supersaturated conditions at specific locations even while the volume-averaged properties of the system remained undersaturated.

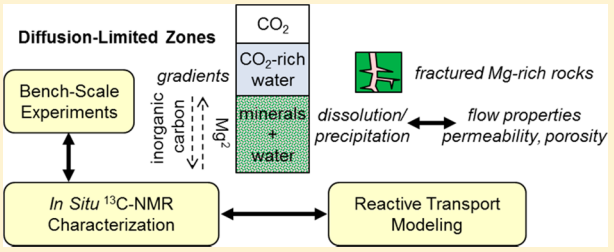

INTRODUCTION

Geologic carbon sequestration (GCS) is a promising strategy for mitigating the impacts of anthropogenic CO_2 emissions on global climate change. GCS involves the injection of CO_2 as a supercritical fluid at high pressures and temperatures into deep geologic formations. The ultimate fate of the carbon within the storage zone includes free supercritical CO_2 trapped within pores and beneath capping formations, CO_2 dissolved in the water, and carbonate minerals formed upon CO_2-water-rock reactions.[1,2] Most geologic formations currently used or proposed for carbon sequestration are sandstone and carbonate saline aquifers and depleted oil and gas reservoirs.[1,3] These formations are attractive for GCS because they have porosity and permeability that facilitate injection of CO_2, but they have limited capacities for mineral trapping because of the low contents of silicate minerals that contain the Ca, Mg, and Fe necessary for carbonate mineral formation. However, Fe- and Mg-rich (ultramafic) basalt and peridotite formations are potential alternative target systems that can provide extensive mineral carbonation.[4,5] Reactive transport modeling simulations found that 100% of the CO_2 could be immobilized within 10 years by mineral trapping for pilot-scale CO_2 injection into basalts.[6] Further the formation of carbonate minerals in olivine-rich peridotites may be self-enhancing from fractures induced by carbonate precipitation and by the exothermic nature of the overall process.[7,8] Other recent simulations have explicitly considered the trade-offs between mineral trapping potential and porosity and permeability for volcanogenic sandstones with higher-than-average iron and magnesium contents for sandstones, and these concluded that 80% of CO_2 could be mineralized within 1000 years.[9]

Release of Mg^{2+}, Ca^{2+}, or Fe^{2+} from silicate minerals followed by precipitation of carbonate minerals that contain those divalent cations are the dominant reactions involved in mineral trapping. Forsterite (Mg_2SiO_4), which is the Mg end member of olivine ($Mg_xFe_{2-x}SiO_4$), is abundant in peridotites and basalts and has consequently been extensively studied with respect to its reaction with CO_2 at high pressures and temperatures. Forsterite dissolution, which is faster at low pH,[10] is accelerated by the low pH provided by high pressure CO_2. The forsterite releases Mg^{2+} to solution, and its dissolution also results in an increase in pH that increases the concentration of CO_3^{2-} for fixed P_{CO2} conditions. Ultimately, the solution becomes sufficiently supersaturated to initiate precipitation of magnesium carbonate minerals. Magnesite ($MgCO_3$) is the dominant end product of mineral trapping observed at the high temperatures (~100 °C) that would be

Received: August 18, 2014
Revised: October 26, 2014
Accepted: November 17, 2014
Published: November 25, 2014

encountered in GCS sites.[11−13] At lower temperatures, nesquehonite ($MgCO_3 \cdot 3H_2O$) is often observed,[14,15] although magnesite precipitation has also been observed in wet supercritical CO_2 at lower temperatures (35 °C).[12]

Silicate mineral dissolution and carbonate mineral formation have been observed in laboratory studies with monolithic rock samples. These studies are important extensions of the work with forsterite, which is primarily done using fine-grained powders. Postreaction characterization of rock samples determined that the microstructure exerts strong control over the extent of mineral trapping. With peridotite cores, silicate dissolution occurs primarily along fractures, and carbonate minerals partially fill those zones.[16] Carbonate deposition that fills pore space of a fractured peridotite cube was observed as well as a carbonate layer at the surface of the cube.[17,18] Precipitation of Ca−Mg−Fe carbonates, which were frequently poorly crystalline, was also observed in reactions of basalt samples reacted at high CO_2 pressure at temperatures below 100 °C.[19,20]

Diffusive mass transfer in materials like the fractured basalts and peridotites can give rise to strong geochemical gradients. The mobile CO_2-rich water in advectively connected fractures will have a low pH, a high dissolved inorganic carbon content (DIC), and a low Mg concentration. Within unconnected or dead-end fractures, the pH and Mg concentration can be higher, but the DIC will be lower. The opposing gradients in pH, Mg, and DIC may lead to highly localized development of supersaturated conditions that result in magnesium carbonate precipitation.

In addition, the filling of fractures with carbonate minerals in intact peridotite and basalt rocks raises questions as to whether such fracture filling might clog pores to such an extent that large portions of reactive minerals like olivine are no longer available for mineral trapping. Any alterations of porosity or permeability caused by geochemical reactions might then further affect local geochemistry through coupled feedback mechanisms.

The objective of this study was to evaluate the effect of diffusive transport limitations on the timing and spatial localization of magnesium carbonate precipitation in a forsterite-CO_2-water system at pressure and temperature conditions relevant to GCS. This objective was pursued by integrating a bench-scale reactive tube experiment with ex situ characterization, in situ characterization of mineral trapping by ^{13}C nuclear magnetic resonance (NMR) spectroscopy, and reactive transport modeling. An ancillary objective was to assess the degree to which these complementary approaches yielded similar predictions or observations of mineral trapping.

MATERIALS AND METHODS

Tubular Reactor Experiments. Commercial forsterite powder, with a size fraction of 10−44 μm, was purchased (Alfa Aesar) for use in experiments. The as-received material was treated by five sequences of sonication in ethanol followed by settling to remove any adhered particles smaller than 10 μm. The treated powder was rinsed in ultrapure water and dried prior to use in the experiments. The specific surface area (SSA) of the powder was determined to be 1.38 m^2/g by BET-N_2 adsorption. This value corresponds to hard spheres with a diameter of 2.6 μm, which indicates that the surface area is influenced either by particles finer than 10 μm that were still present after treatment or by high surface roughness. Powder X-ray diffraction (XRD) was used to confirm the crystalline structure as forsterite.

The overall reactor consisted of a well-mixed batch system with 200 mL of water and 100 mL of headspace CO_2 with a tube packed with forsterite and open at one end immersed in this well-mixed CO_2-rich solution (Figure 1). While the bulk

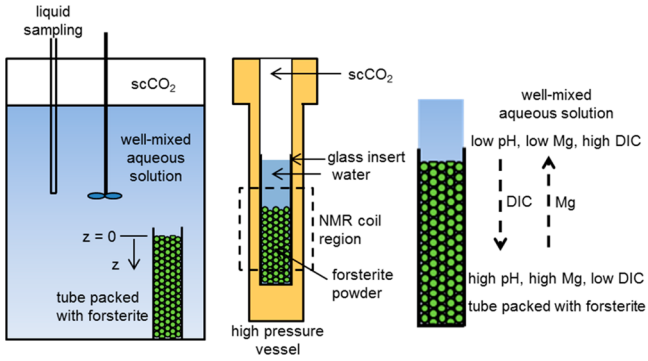

Figure 1. Experimental systems for forsterite dissolution in a tubular reactor (left), a high pressure zirconia reaction vessel for in situ ^{13}C NMR measurements (center), and a schematic of the packed tube of forsterite with the diffusive mass transfer of inorganic carbon and magnesium noted (right).

solution was well-mixed by an overhead stirrer, the solution within the tube was stagnant. This configuration allowed chemical gradients to develop along the length of the tube with CO_2 concentrations being highest and the pH lowest at the open end of the tube. Tests using a glass beaker in place of the reactor body but with the same mixing speed confirmed that the particles in the packed bed were not mobilized by the mixing of the bulk solution; consequently diffusion and possibly some dispersion from convection, but not enough to mobilize fine particles, were the only processes by which solutes could transfer into or out of the tube. The source of magnesium for magnesite precipitation was the forsterite in the tube. Forsterite dissolution releases Mg^{2+} and causes the pH to increase. The dissolved Mg^{2+} can then diffuse along the length of the tube, with a net flux out of the tube, or precipitate in secondary minerals. Borosilicate glass tubes (0.64 cm diameter and 7.5 cm length, Fisher Scientific), were wet packed with the forsterite powder to a depth of 5.5 cm. Using the measured mass of the forsterite loaded into the tube, the dimensions of the tube, and the known density of forsterite, the porosity of the packed bed was calculated to be 0.44 based on the measured volume and mass and the known density of forsterite. After the tube was loaded with forsterite it was fixed in place by attachment to the head of a high pressure reactor at a location that would keep the top of the tube fully submerged once the reactor was loaded with water and sealed. The reactor head was connected to a stainless steel reactor body that included a PTFE liner that was loaded with 200 mL of ultrapure water (resistivity >18.2 MΩ·cm).

After the whole reactor was assembled, the temperature was increased to 100 °C and maintained with a heating mantle and a headspace CO_2 pressure was maintained at 100 bar using a high-pressure syringe pump (Isco Teledyne). Because this was the temperature of the entire reactor, there would not be any temperature gradients within the reactor that would give rise to convective mixing. The temperature was reached within 30 min and the headspace CO_2 was achieved within minutes. While it

will take more time for equilibration of the headspace CO_2 and the aqueous solution, the time scale for that equilibration is still much shorter than that of the mass transfer processes that give rise to chemical gradients within the tube. At 100 °C and 100 bar, the CO_2 in the headspace is present as a supercritical fluid. The water is then equilibrated with the CO_2 and remains at constant $CO_{2(aq)}$. As determined using the speciation model discussed below, the pH will be 3.2 and the DIC concentration 0.78 M at these conditions. Although 100 °C is higher than what would be encountered at a depth that would correspond to 100 bar in most geologic formations, the temperature accelerated reactions and allowed greater extents of reaction to be observed over experimentally tractable time-scales. In ultramafic formations, the exothermic nature of the carbonation reaction can also lead to temperatures greater than those prior to CO_2 injection.[8] Separate experiments were operated for periods of 1, 3, 5, and 14 days before the tube was retrieved for ex situ characterization.

Raman spectroscopy was used to probe for magnesium carbonate precipitation along the length of the tube. Using a laser microprobe, the spectra could be collected through the glass walls of the tube, but higher quality spectra were obtained when analyzing 1 cm increments of the solids from the tube after they had been removed and homogenized to minimize variation in carbonate content across the cross section of the bed. The Raman measurements were made with a HoloLab Series 5000 laser raman microprobe (Kaiser Optical) that delivered a 532 nm laser beam from a frequency-doubled Nd:YAG laser through a 20× -working-distance objective with a 0.4 numerical aperture. This configuration delivered a maximum of 11 mW of laser power onto the sample. The 1 cm increments of the solids were also analyzed by powder XRD in a method with identical preparations of the same mass of solids from each increment to enable semiquantitative analysis of variations in secondary mineral quantities with depth. XRD patterns were collected using a Rigaku Geigerflex D-MAX/A Diffractometer with Cu-Ka radiation.

^{13}C NMR Measurements. The reactions of forsterite in CO_2-rich aqueous solution were tracked in situ using a high-temperature, elevated-pressure ^{13}C NMR probe (Figure 1) that has been described previously.[21] This top loading probe is used in an 8.3T magnet with an NMR circuit specifically tuned to the resonance frequency of ^{13}C at 89.066745 MHz. Typical conditions included data acquisition through 16 row phase cycled spin echo experiments with typical $\pi/2$ pulse lengths of 16 μs, using recycle delays of 60 s and recording 128 transients. ^{13}C NMR signals were referenced to CO_2 gas (at 125 ppm). The probe includes a glass liner for holding the sample within a yttria-stabilized zirconia reaction vessel that is 14 cm long and has an inner diameter of 1.0 cm. Heating was provided by blowing heated air across the vessel, and the temperature was monitored at two locations with Type K thermocouples. Pressure was provided by condensing known amounts of CO_2 at liquid nitrogen temperatures in a stainless steel tube, and then allowing that CO_2 to evaporate in a closed system connected to the reaction vessel. A pressure transducer continuously monitored the pressure.

An experiment was performed at 80 °C and 105−120 bar CO_2 to study CO_2-water-forsterite reactions. Labeled $^{13}CO_2$ was used to track the dissolution of CO_2 into the water, its conversion to $H^{13}CO_3^-$ and ultimately its precipitation as carbonate solids. The reaction vessel was loaded with forsterite powder (Alfa Aesar) to form a bed that was then saturated with water with some free water kept above the forsterite bed. Static ^{13}C NMR spectra of the mineral-loaded reactor were collected regularly over the course of a 21 day experiment.

Reactive Transport Model. A reactive transport model was developed to simulate the chemical gradients that would develop along the length of the packed bed as CO_2 diffused into the tube, forsterite dissolved, and magnesium diffused out of the tube. The model consisted of linked mole balance equations for the tubular reactor and for the bulk solution. The boundary condition for the open end of the bed was that the conditions were the same as in the 200 mL well-mixed solution. The dissolved CO_2 concentration in the well-mixed solution was fixed based on equilibrium with the fixed 100 bar headspace of CO_2 and calculated using the equations of state of Sterner and Pitzer[22] and the solubility equations of Duan and Sun.[23,24] The total dissolved inorganic carbon and dissolved Mg and Si in the well-mixed system increased as the experiment progressed; at these pH values the dominant dissolved species are Mg^{2+} and H_4SiO_4. Forsterite dissolution was the only kinetically controlled reaction considered in the model. All other reactions were considered to be at local equilibrium. Those reactions and their equilibrium constants at 100 °C and 100 bar are summarized in Table 1.

Table 1. Equilibrium Constants and Solubility Products for Related Chemical Reactions at100 °C and 100 bar CO_2 pressure

reactions	log K^a at 100 °C and 100 bar P_{CO2}
$CO_{2(aq)}$ (molal)^b	0.79
$H_2O = H^+ + OH^-$	−12.22
$H_2O + CO_{2(aq)} = H^+ + HCO_3^-$	−6.35
$H_2O + CO_{2(aq)} = 2H^+ + CO_3^{2-}$	−16.38
$MgCO_{3(s)} = Mg^{2+} + CO_3^{2-}$	−9.41
$SiO_{2(am)} = SiO_{2(aq)}$	−2.16
$Mg_2SiO_{4(s)} + 4H^+ = 2Mg^{2+} + SiO_{2(aq)} + 2H_2O$	20.51

^{a}All values, except $CO_{2(aq)}$, were calculated using SUPCRT92 with the dSLOP98 database. ^{b}$CO_{2(aq)}$ concentration is a fixed value when the aqueous phase is at equilibrium with a headspace at fixed 100 °C and 100 bar P_{CO2}. Calculations were made using the equations of state of Sterner and Pitzer[22] and the solubility equations of Duan et al.[23,24]

Mole balance equations were included for dissolved Mg, Si, and inorganic carbon. The mole balance equations for dissolved Mg inside the tubular reactor and the batch reactor are shown in eqs 1 and 2.

$$\frac{\partial c_{Mg,t}}{\partial t} = D_{Mg}\frac{\partial^2 c_{Mg,t}}{\partial z^2} + R_{Mg,Fo} \quad (1)$$

$$V_b\frac{\partial c_{Mg,b}}{\partial t} = -D_{Mg}\frac{\partial c_{Mg,t}}{\partial z}_{z=0}\cdot S_t\cdot\varepsilon \quad (2)$$

The dissolved Mg concentrations in the tubular reactor and well-mixed batch solution are $C_{Mg,t}$ and $C_{Mg,b}$ (mol/cm^3), respectively. D_{Mg} (cm^2/s) is the diffusivity of Mg^{2+} in the aqueous phase. V_b is the solution volume (cm^3) in the batch reactor, S_t (cm^2) is the cross-sectional area of the tubular reactor, and ε is the porosity of the packed bed. Table 2 summarizes all of the parameters used in the modeling and their values. $R_{Mg,Fo}$ (mol/cm^3-s) is the rate of Mg addition to the solution from forsterite dissolution. A pH-dependent

Table 2. Parameters Included for Reactive Transport of Dissolved Mg and Inorganic Carbon

parameters	value
tube length (L)	5.51 cm
tube diameter (D)	0.635 cm
volume of batch reactor (V_b)	200 cm^3
porosity (ϕ)	0.44
density of forsterite (ρ_{Fo})[a]	3.2 g/cm^3
radius of forsterite particle[b]	2.6×10^{-4} cm
diffusivity of Mg^{2+} (D_{Mg})[c]	$2.369 \times 10^{-8} \bullet T$ (K) (cm^2/s)
diffusivity of dissolved CO_2 (D_{CO2})[c]	3.03×10^{-5} cm^2/s assumed for 100 °C.

[a]The density is that of the forsterite solids. [b]The radius of forsterite particle was calculated by assuming all the particles were spheres with the same radius and a specific surface area of 1.38 m^2/g. [c]Taken from Newman and Thomas-Alyea.[36]

dissolution rate (mol/cm^2-s) for forsterite (eq 3) was taken from a recent critical synthesis of previous dissolution rate measurements.[10]

$$\log r = 6.05 - 0.46\text{pH} - \frac{3683}{T}, \text{ pH} < 5.6$$
$$= 4.07 - 0.256\text{pH} - \frac{3465}{T}, \text{ pH} > 5.6 \quad (3)$$

$R_{Mg,Fo}$ was then calculated from information regarding the rate of forsterite dissolution, bed porosity, and the specific surface area of the forsterite. Similar mole balance equations were used for dissolved inorganic carbon, but without the inclusion of the forsterite dissolution term.

Under the constraint of charge balance for the solution, and total dissolved concentrations of Mg, Si, and inorganic carbon, the speciation, including the pH, in the tube was calculated at grid cells along the z direction as a function of time. Ultimately, both the magnesium and inorganic carbon mole balance equations would be affected by magnesium carbonate precipitation; however, the primary goal of the modeling in this study was to identify the timing and location of initial magnesium carbonate precipitation, which was accomplished by determining the saturation index of the solution in the tube with respect to magnesite. In particular the modeling was used to evaluate whether or not the spatial localization of magnesite precipitation could be explained by gradients in the concentrations of Mg and DIC.

At the open end of the tubular reactor ($z = 0$), the dissolved Mg concentration is always the same as that in the well-mixed solution of the batch reactor. This concentration will increase over time, but because of the very high solid−water ratios within the tube, the concentrations within the tube will be much larger than those in the well-mixed outer solution. At the closed end of the tubular reactor ($z = L$), the flux of Mg is zero. The initial Mg concentrations in both the tubular reactor and the batch reactor were set to zero under the assumption that no forsterite had dissolved yet. A sensitivity analysis found that the final simulation results were not sensitive to this initial condition, and similar final results were achieved if an initial condition of water in the tube equilibrated with forsterite was used.

The numerical solution procedure involved decoupling the transport process and the chemical reactions. Diffusive transport was discretized with second-order accuracy using time and space steps required for stability of the equations. Then at each location and time, the chemical reactions were solved to determine the local pH and speciation of dissolved inorganic carbon, magnesium, and silicon. A custom-built code was written in C++ for the solution of the equations.

RESULTS AND DISCUSSION

Ex Situ Characterization of Solids from the Tubular Reactor. Magnesium carbonate precipitation was detectable after 5 days of reaction with maximum amounts of precipitation located 1.0 cm (±0.3 cm) from the interface of the forsterite packed bed with the well-mixed batch solution (z = 1 cm). The semiquantitative XRD analysis has peaks characteristic of magnesite near 32° and 43° (2θ) that have the greatest relative peak areas to the forsterite peaks at a depth of 1 cm (Figure 2).

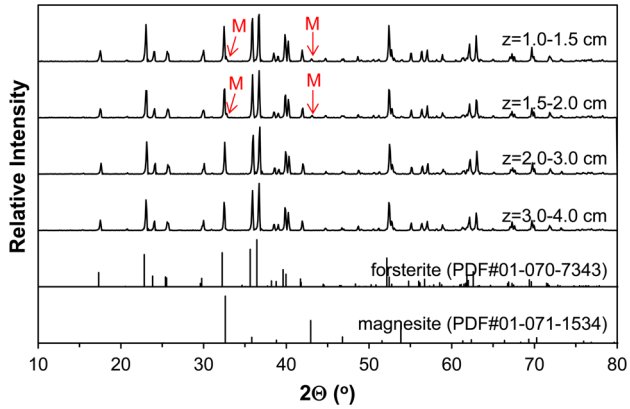

Figure 2. X-ray diffraction patterns of solids along the length of the tubular reactor for solids reacted for 5 days at 100 °C and 100 bar CO_2. Reference patterns for forsterite and magnesite are included for comparison. Diagnostic peaks for magnesite are denoted with "M" and the arrows.

It is possible that magnesite precipitation was accompanied by the formation of other magnesium carbonates. Recent work observed predominant nesquehonite precipitation in solutions equilibrated with 90 atm CO_2 with magnesite only observed at the highest temperature studied (80 °C),[25] and earlier work observed a strong effect of pressure and temperature on the identity of the carbonate mineral formed with magnesite being the principal phase at 120 °C and 100 bar CO_2.[13] Iron from either the reactor or from trace amounts in the forsterite could also facilitate carbonate precipitation.[26] The 5-day experiment was the first one in which detectable amounts of carbonate minerals were present; no detectable peaks were present in the 1-day and 3-day samples. The spatial localization of magnesite precipitation can be caused by the opposing gradients in dissolved magnesium and dissolved inorganic carbon within the tubular reactor. Magnesite precipitation requires both magnesium from within the tube and inorganic carbon, which is diffusing in from the well-mixed solution. These gradients in concentration together with the pH gradient that results from instantaneous local equilibration of the solution will create solutions that achieve critical supersaturation with respect to magnesite at a particular time and location. The concentrations of both magnesium and dissolved inorganic carbon in the tube increase with time, and 5 days must be sufficient to have achieved a solution that is sufficiently supersaturated at 1 cm to facilitate nucleation. At shallower depths in the bed the solution supersaturation is lower. A recent microfluidic flow-through

dx.doi.org/10.1021/es504047t | Environ. Sci. Technol. 2014, 48, 14344−14351

study of forsterite reactions with CO_2-rich water found that magnesite only precipitated in diffusion-limited zones and not along primary flow channels.[27]

A depth profile using Raman spectroscopy of solids from the 5-day experiment also did not observe any magnesium carbonates until a depth of 1 cm (Figure 3). While magnesite

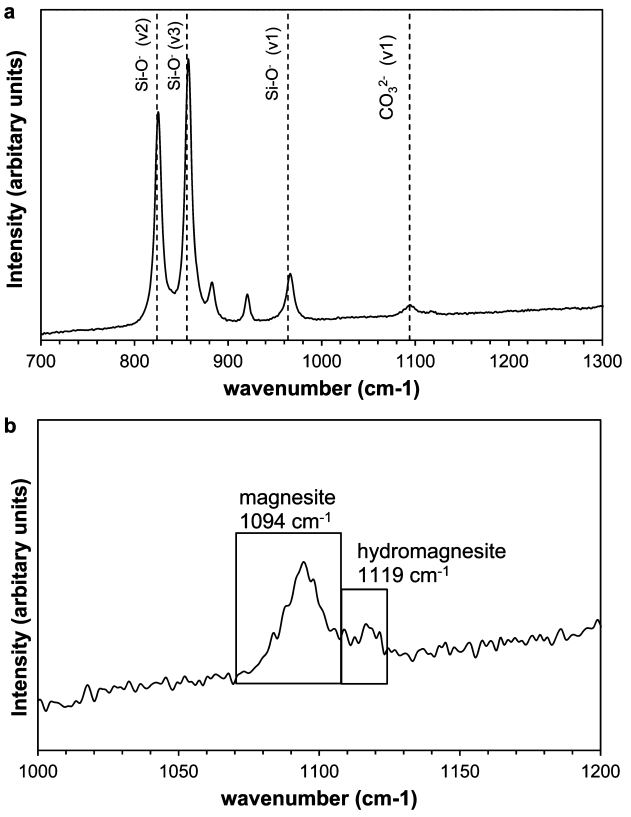

Figure 3. Raman spectra from 1 cm into the tube after 5 days of reaction at 100 °C and 100 bar P_{CO2} shown for the range that includes (a) Si−O and CO_3^{2-} stretches and (b) higher resolution of the CO_3^{2-} stretch region. Peak assignments are included with the three major bands at 964, 855, and 824 cm^{-1} from Si−O vibrations associated with forsterite and peaks at 1094 and 1119 cm^{-1} from magnesite and hydromagnesite, respectively.

was the only solid that could be detected with XRD, the greater sensitivity of Raman spectroscopy allowed the observation of small amounts of hydromagnesite as well. A related study with a different size and composition of forsterite also observed spatial localization of maximum amounts of magnesite carbonate precipitation; both magnesite and hydromagnesite formed, but magnesite was the only detectable phase after 8 days of reaction.[28] The bands at 1094 and 1119 cm^{-1} are assigned to the symmetric CO_3^{2-} stretching in magnesite, and hydromagnesite, respectively.[29] The three bands at 964, 855, and 824 cm^{-1} wavenumbers are indicative of the Si−O stretching modes of forsterite.[30] Hydromagnesite is a known intermediate for magnesite precipitation.[13] Raman spectroscopy experiments performed with finer grained forsterite (5−40 μm) and a 3 cm deep bed also observed formation of hydromagnesite followed by magnesite; carbonate minerals were first detected after 1 day at a depth of 0.5 cm.[28] Total carbon analyses in that related study observed a maximum amount of carbonate precipitation at 0.5 cm into the packed bed.

^{13}C NMR Measurements. The in situ ^{13}C NMR data provide information on the evolution of inorganic carbon in both the aqueous and solid phase. The NMR signal from the initial supercritical $^{13}CO_2$ at a chemical shift of 128 ppm declines over time as the $^{13}CO_2$ dissolves into the water, the inorganic carbon reacts, and is all but gone after 13 h. With time the spectra also indicate a concomitant increase of $CO_{2(aq)}$ and HCO_3^- at 126 and 161.5 ppm, respectively (Figure 4). The

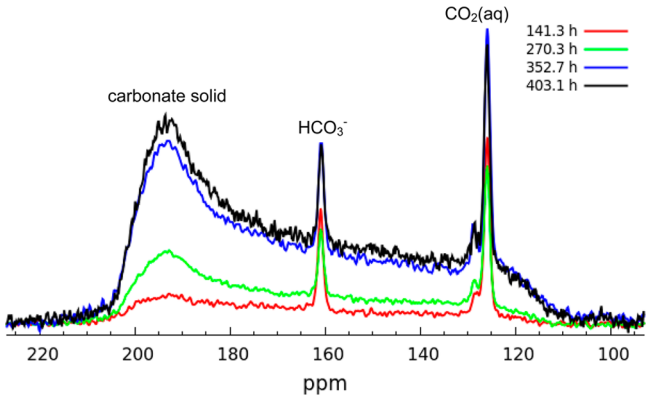

Figure 4. In situ ^{13}C NMR monitoring of reaction progress at 80 °C and 105−120 bar $^{13}CO_2$ for a bed of forsterite with water filling the pores. Spectra were recorded at each of the times indicated in the legend. The broad resonance extending from 205 to 110 ppm is from mineral carbonates, primarily magnesite. A small supercritical-CO_2 signal can be seen as a peak beside that of the CO_2(aq) resonance, due to a small amount of the former being introduced between the high-pressure sample holder and the glass tube holding the bed of forsterite.

broad peak at 190 ppm is from magnesite and shows a shape characteristic of a broad axially symmetric chemical shift anisotropy (CSA) powder pattern.[31] This broad resonance is barely discernible after 141 h (5.9 days), and then it increases significantly with continuing reaction. The timing of first observable magnesite precipitation is very similar to that observed for the solids from the tubular reactor by ex situ characterization. The ^{13}C NMR spectra would be sensitive to transformations of hydromagnesite to magnesite if there were sufficient signal from each species present to distinguish the two, but under these conditions (especially at later reaction times) magnesite was the only detectable solid. This observation agrees with a lifetime of hydromagnesite observed previously for similar conditions using ^{13}C HP-MAS NMR.[32]

Reactive Transport Modeling. Simulations using the reactive transport model predict the development of strong chemical gradients along the length of the tubular reactor. The gradient in the Mg concentration is sharpest in the first 2 cm into the tube (Figure 5a), and at the closed end of the tube the Mg concentration increases until reaching 0.08 M after 7 days (168 h). A peak in the Mg concentration develops because the dissolution of forsterite, which is the source of the dissolved magnesium, is faster at the lower pH values near the open end of the tube. Magnesium can diffuse both out of the tube and deeper into the tube from this peak, but the large gradient in concentration between the peak and the bulk solution outside of the tube lead to a net flux of Mg out of the tube. The Mg concentration at the very top of the tube is required to be the same as that in the bulk solution; although the concentration in the bulk solution is increasing because of Mg release from the tube, the concentrations achieved are orders of magnitude

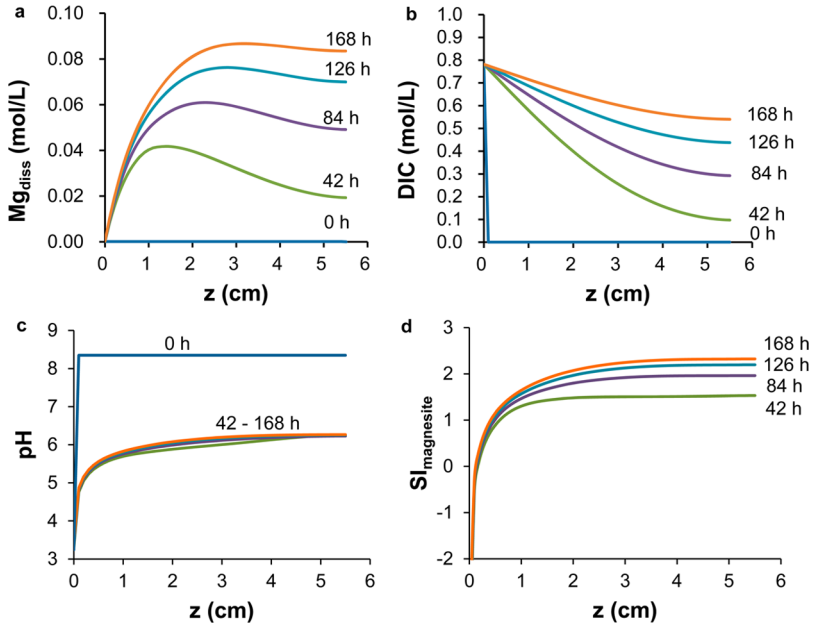

Figure 5. Simulated profiles of (a) the Mg concentration, (b) DIC concentration, (c) pH, (d) and saturation index for magnesite (SI_{mag}) inside the tubular reactor loaded with forsterite and operated at 100 °C and 100 bar CO_2 for reaction times up to 1 week (168 h).

lower than those within the tube. The concentration of DIC also gradually increases at deeper regions of the tube, and its gradient also remains sharpest in the shallowest zones of the tube (Figure 5b). The combination of total Mg and inorganic carbon concentrations yields local pH values that increase from about 3.2 at the open end of the tube (where the pH is dominated by the acidity from the dissolved CO_2) to almost 5.6 deeper into the tube where the pH is controlled by both the CO_2 injection and the neutralization of the acidity from the dissolution of forsterite (Figure 5c).

For all reaction times plotted, the saturation index increases markedly with distance into the tube going from unfavorable to favorable conditions for magnesite saturation. This increase is driven by the gradients in pH, DIC, and dissolved Mg. The gradient in saturation index is consistent with spatial localization of magnesite precipitation, since magnesite would be expected to first precipitate and then grow at the location at which a critical saturation index for nucleation is first achieved. A saturation index of approximately 1.6 for magnesite is calculated from the model output at the experimentally observed time (5 days) and location (1 cm) of initial magnesite precipitation. The saturation index is calculated using the concentrations of dissolved Mg^{2+} and CO_3^{2-} and associated activity coefficients determined with the Davies equation. The CO_3^{2-} concentration is determined from the pH and dissolved inorganic carbon concentration (Figure 5d). Previous experiments at 100 °C and 100 bar with the well-mixed reactor found that a critical saturation index of 2.0 was necessary to overcome the nucleation barrier to magnesite formation.[33] This is higher than an earlier critical saturation index range of 0.25−1.14 determined at 100 °C in a different reactor configuration, but those experiments were at a lower CO_2 pressure.[34] The timing and localization of magnesite precipitation simulated by the model is qualitatively consistent with the experimental measurements. This consistency was achieved for a model whose parameters were determined from the literature and not from any fitting of the simulations to the experimental data. While the model predicts that with time deeper zones of the tube will become even more supersaturated, precipitation of magnesite at the initial sites of nucleation would sequester the magnesium and could limit the extent of precipitation deeper in the tube. The current version of the model did not include a reaction for magnesium carbonate precipitation so it can only predict the location and timing of precipitation and not the evolution of the bed composition after precipitation starts. Future refinements of the model can account for the precipitation of magnesium carbonates as well as Mg-containing minerals such as smectites. The model may also be improved by explicitly considering the mole balance for silicon in the system since dissolved silicon can lead to surface phases that inhibit dissolution of forsterite,[11,35] including phases whose formation is facilitated by the presence of iron.[26]

Environmental Implications. Unlike in well-mixed experiments that are often done to quantify reaction rates and mechanisms of CO_2-water-mineral reactions, actual geologic carbon sequestration will take place in porous or fractured media that are not well-mixed. In these systems zones in which mass transfer is limited to diffusion can have local geochemical conditions that are very different from volume-averaged properties. The experiments and modeling in this study demonstrate that mineral carbonation can occur in such diffusion-limited zones well before volume-averaged properties of the system have reached saturation with respect to magnesite precipitation. Accounting for local geochemical conditions, especially pH since it controls the rates of many reactions, in simulations of GCS environments is important for developing accurate predictions of the fate of injected CO_2.

The experiments in this study illustrate that carbonate mineral formation can be highly localized in diffusion-limited zones. The extent to which this precipitation clogs pores and inhibits CO_2 reactions with mineral surfaces below the zone of maximum precipitation may control the overall mineral trapping capacity of a geologic formation. Further research is needed to examine the feedback between dissolution−precipitation reactions and transport properties for such diffusion-limited systems. The approach of integrated tubular

reactor experiments, in situ spectroscopic characterization, and reactive transport modeling can be extended to study such coupling both for magnesium-rich rocks and other diffusion-limited zones such as those that are present in caprocks.

AUTHOR INFORMATION

Corresponding Author

*Phone: (314) 935-6849; fax: (314) 935-7211; e-mail: giammar@wustl.edu.

Present Address

[‖]PPG, Pittsburgh, Pennsylvania.

Notes

The authors declare no competing financial interest.

ACKNOWLEDGMENTS

This research was supported by the Consortium for Clean Coal Utilization at Washington University. The idea for the tubular reactor experiments originated from discussions with Anurag Mehra, and Dr. Mehra and Sachin Godbole made initial efforts toward reactive transport modeling. Giammar is grateful for the Kenan Visiting Professorship at Princeton University that facilitated the integration of the experiments and modeling. Heather Hunter implemented the use of activity coefficients in the reactive transport model. Wei Xiong and Jeremy Moore provided assistance with experiments.

REFERENCES

(1) IPCC, *IPCC Special Report on Carbon Dioxide Capture and Storage*; Cambridge University Press: Cambridge, UK, 2005.

(2) Jun, Y. S.; Giammar, D. E.; Werth, C. J. Impacts of geochemical reactions on geologic carbon sequestration. *Environ. Sci. Technol.* **2013**, *47* (1), 3−8.

(3) Kevitiyagala, N. Carbon sequestration. *Science* **2012**, *325* (5948), 1644−1645.

(4) Goff, F.; Lackner, K. S. Carbon dioxide sequestering using ultramafic rocks. *Environ. Geosci.* **1998**, *5* (3), 89−102.

(5) Matter, J. M.; Kelemen, P. B. Permanent storage of carbon dioxide in geological reservoirs by mineral carbonation. *Nat. Geosci* **2009**, *2* (12), 837−841.

(6) Aradottir, E. S. P.; Sonnenthal, E. L.; Bjornsson, G.; Jonsson, H. Multidimensional reactive transport modeling of CO_2 mineral sequestration in basalts at the Hellisheidi geothermal field, Iceland. *Int. J. Greenhouse Gas Control* **2012**, *9*, 24−40.

(7) Matter, J. M.; Kelemen, P. B. Enhanced in situ carbonation of peridotite for permanent CO_2 storage. *Geochim. Cosmochim. Acta* **2009**, *73* (13), A848−A848.

(8) Kelemen, P. B.; Matter, J. In situ carbonation of peridotite for CO_2 storage. *Proc. Natl. Acad. Sci. U. S. A.* **2008**, *105* (45), 17295−17300.

(9) Zhang, S.; DePaolo, D. J.; Xu, T. F.; Zheng, L. G. Mineralization of carbon dioxide sequestered in volcanogenic sandstone reservoir rocks. *Int. J. Greenh Gas Con* **2013**, *18*, 315−328.

(10) Rimstidt, J. D.; Brantley, S. L.; Olsen, A. A. Systematic review of forsterite dissolution rate data. *Geochim. Cosmochim. Acta* **2012**, *99*, 159−178.

(11) Sissmann, O.; Daval, D.; Brunet, F.; Guyot, F.; Verlaguet, A.; Pinquier, Y.; Findling, N.; Martinez, I. The deleterious effect of secondary phases on olivine carbonation yield: Insight from time-resolved aqueous-fluid sampling and FIB-TEM characterization. *Chem. Geol.* **2013**, *357*, 186−202.

(12) Felmy, A. R.; Qafoku, O.; Arey, B. W.; Hu, J. Z.; Hu, M.; Schaef, H. T.; Ilton, E. S.; Hess, N. J.; Pearce, C. I.; Feng, J.; Rosso, K. M. Reaction of water-saturated supercritical CO_2 with forsterite: Evidence for magnesite formation at low temperatures. *Geochim. Cosmochim. Acta* **2012**, *91*, 271−282.

(13) Hanchen, M.; Prigiobbe, V.; Baciocchi, R.; Mazzotti, M. Precipitation in the Mg-carbonate system—Effects of temperature and CO_2 pressure. *Chem. Eng. Sci.* **2008**, *63* (4), 1012−1028.

(14) Case, D. H.; Wang, F.; Giammar, D. E. Precipitation of magnesium carbonates as a function of temperature, solution composition, and presence of a silicate mineral substrate. *Environ. Eng. Sci.* **2011**, *28* (12), 881−889.

(15) Thompson, C. J.; Loring, J. S.; Rosso, K. M.; Wang, Z. M. Comparative reactivity study of forsterite and antigorite in wet supercritical CO_2 by in situ infrared spectroscopy. *Int. J. Greenhouse Gas Control* **2013**, *18*, 246−255.

(16) van Noort, R.; Spiers, C. J.; Drury, M. R.; Kandianis, M. T. Peridotite dissolution and carbonation rates at fracture surfaces under conditions relevant for in situ mineralization of CO_2. *Geochim. Cosmochim. Acta* **2013**, *106*, 1−24.

(17) Hovelmann, J.; Austrheim, H.; Jamtveit, B. Microstructure and porosity evolution during experimental carbonation of a natural peridotite. *Chem. Geol.* **2012**, *334*, 254−265.

(18) Hovelmann, J.; Austrheim, H.; Beinlich, A.; Munz, I. A. Experimental study of the carbonation of partially serpentinized and weathered peridotites. *Geochim. Cosmochim. Acta* **2011**, *75* (22), 6760−6779.

(19) Gysi, A. P.; Stefansson, A. Experiments and geochemical modeling of CO_2 sequestration during hydrothermal basalt alteration. *Chem. Geol.* **2012**, *306*, 10−28.

(20) Gysi, A. P.; Stefansson, A. CO_2-water-basalt interaction. Low temperature experiments and implications for CO_2 sequestration into basalts. *Geochim. Cosmochim. Acta* **2012**, *81*, 129−152.

(21) Surface, J. A.; Skemer, P. A.; Hayes, S. E.; Conradi, M. S. In situ measurement of magnesium carbonate formation from CO_2 using static high pressure and temperature ^{13}C NMR. *Environ. Sci. Technol.* **2013**, *47*, 119−125.

(22) Sterner, M. S.; Pitzer, K. S. An equation of state for carbon dioxide valid from zero to extreme pressures. *Contributions in Mineralogy and Petrology* **1994**, *117*, 362−374.

(23) Duan, Z.; Sun, R. An improved model calculating CO_2 solubility in pure water and aqueous NaCl solutions from 273 to 533 K and from 0 to 2000 bar. *Chem. Geol.* **2003**, *193*, 257−271.

(24) Duan, Z. H.; Sun, R.; Zhu, C.; Chou, I. M. An improved model for the calculation of CO_2 solubility in aqueous solutions containing Na^+, K^+, Ca^{2+}, Mg^{2+}, Cl^-, and SO_4^{2-}. *Mar Chem.* **2006**, *98* (2−4), 131−139.

(25) Qafoku, O.; Hu, J. Z.; Hess, N. J.; Hu, M. Y.; Ilton, E. S.; Feng, J.; Arey, B. W.; Felmy, A. R. Formation of submicron magnesite during reaction of natural forsterite in H_2O-saturated supercritical CO_2. *Geochim. Cosmochim. Acta* **2014**, *134*, 197−209.

(26) Saldi, G. D.; Daval, D.; Morvan, G.; Knauss, K. G. The role of Fe and redox conditions in olivine carbonation rates: An experimental study of the rate limiting reactions at 90 and 150 degrees C in open and closed systems. *Geochim. Cosmochim. Acta* **2013**, *118*, 157−183.

(27) Yang, L.; Steefel, C. I.; Bechtel, H. In *Microfluidic and Capillary Tube Experimental Study of Forsterite Carbonation by CO_2 Bearing Fluids*, American Geophysical Union Fall Meeting, 2013.

(28) Xiong, W.; Giammar, D. E. Forsterite carbonation in zones with transport limited by diffusion. *Environ. Sci. Technol. Lett.* **2014**, *1*, 333−338.

(29) Edwards, H. G. M.; Villar, S. E. J.; Jehlicka, J.; Munshi, T. FT-Raman spectroscopic study of calcium-rich and magnesium-rich carbonate minerals. *Spectrochim. Acta A* **2005**, *61* (10), 2273−2280.

(30) Mohanan, K.; Sharma, S. K.; Bishop, F. C. A raman spectral study of forsterite-monticellite solid-solutions. *Am. Mineral.* **1993**, *78* (1−2), 42−48.

(31) Lauterbur, P. C. C^{13} nuclear magnetic resonance spectra. *J. Chem. Phys.* **1957**, *26* (1), 217−218.

(32) Kwak, J. H.; Hu, J. Z.; Hoyt, D. W.; Sears, J. A.; Wang, C. M.; Rosso, K. M.; Felmy, A. R. Metal carbonation of forsterite in supercritical CO_2 and H_2O using solid state Si-29, C-13 NMR spectroscopy. *J. Phys. Chem. C* **2010**, *114* (9), 4126−4134.

(33) Wang, F. *Silicate Mineral Dissolution and Associated Carbonate Precipitation at Conditions Relevant to Geologic Carbon Sequestration*. Doctoral Thesis, Washington University, St. Louis, MO, 2013.
(34) Giammar, D. E.; Bruant, R. G., Jr.; Peters, C. A. Forsterite dissolution and magnesite precipitation at conditions relevant for deep saline aquifer storage and sequestration of carbon dioxide. *Chem. Geol.* **2005**, *217*, 257−276.
(35) Daval, D.; Sissmann, O.; Menguy, N.; Saldi, G. D.; Guyot, F.; Martinez, I.; Corvisier, J.; Garcia, B.; Machouk, I.; Knauss, K. G.; Hellmann, R. Influence of amorphous silica layer formation on the dissolution rate of olivine at 90 degrees C and elevated pCO(2). *Chem. Geol.* **2011**, *284* (1−2), 193−209.
(36) Newman, J.; Thomas-Alyea, K. E. *Electrochemical Systems*; John Wiley & Sons, 2004.